P5R.9

SPECTRAL RETRIEVAL OF LATENT HEATING PROFILES FROM TRMM PR DATA: COMPARISON OF LOOK-UP TABLES

Shoichi Shige[1,*] Yukari N. Takayabu[2], Wei-Kuo Tao[3] and Chung-Lin Shie[3,4]

[1]Department of Space Engineering, Osaka Prefecture University, Osaka, Japan
[2]Center for Climate System Research, University of Tokyo, Tokyo, Japan
[3]Laboratory for Atmospheres, NASA/Goddard Space Flight Center, Greenbelt, Maryland, U.S.A.
[4]Goddard Earth Sciences and Technology Center, University of Maryland, Baltimore County, Baltimore, Maryland, U.S.A.

1. INTRODUCTION

The precipitation radar (PR) of the TRMM provides height information based upon the time delay of the precipitation-backscattered return power, and has enabled us to directly obtain vertical profiles of precipitation over the global Tropics (Kozu et al., 2001; Okamoto, 2003). The classification between convective and stratiform regions of mesoscale convective systems (MCS) became more straightforward utilizing observed precipitation profiles (Awaka et al., 1998). The accuracy of this classification is very important for estimating latent heating, because the differences of diabatic heating profiles that exist between convective and stratiform regions of MCSs (Houze, 1982; Johnson and Young, 1983). For convective regions of MCSs the heating profile has warming at all levels with a maximum at midlevels, whereas in stratiform regions there is a warming peak in the upper troposphere and a cooling peak at low-levels. The resulting MCS heating profile is positive at all levels, but with a maximum value in the upper troposphere.

Takayabu (2002) obtained a spectral expression of precipitation profiles to examine convective and stratiform rain characteristics statistically over the equatorial area (10^oN-10^oS) observed by the TRMM PR. In her study, all nadir data of PR2A25 version 5 (Iguchi et al. 2000) for the period of 1998-1999 were utilized and convective and stratiform precipitation were separated based on the TRMM PR version 5 2A23 convective-stratiform separation algorithm. Precipitation profiles with 0.3 mm hr^{-1} precipitation-top threshold were accumulated and stratified with precipitation-top heights (PTHs). Properties of convective rain profiles show near monotonic change with cumulative frequency. Stratiform rain profiles consist of two groups. One group consists of shallow stratiform rain profiles which are very weak and increase downward. The other group consists of anvil rain profiles, characterized by maximum intensity around the melting level, much less intensity above, and a downward decrease below as indicated in traditional radar observations.

Based on the results of spectral precipitation statistics of Takayabu (2002), the Spectral Latent Heating (SLH) algorithm has been developed for the TRMM PR (Shige et al. 2004, hereafter S2004). Heating profile lookup tables for the three rain types– convective, shallow stratiform, and anvil rain (deep stratiform with a melting level) were produced with numerical simulations of tropical cloud systems in Tropical Ocean Global Atmosphere (TOGA) Coupled Ocean–Atmosphere Response Experiment (COARE) utilizing a cloud-resolving model (CRM). For convective and shallow stratiform regions, the lookup table refers to the precipitation top height (PTH). For anvil region, on the other hand, the lookup table refers to the precipitation rate at the melting level instead of PTH.

It is necessary to examine the universality of the lookup table for global application of the SLH algorithm to TRMM PR data. If relationship between precipitation profiles and associated latent heating profiles change between regions, the lookup table would produce large error. In this study, we compare the lookup table from TOGA-COARE, GARP Atlantic Tropical Experiment (GATE), South China Sea Monsoon Experiment (SCSMEX) and Kwajelin Experiment (KWAJEX) simulations to examine its universality.

2. APPROACH

Due to the scarcity of reliable validation data and difficulties associated with the collocation of validation data and satellite measurements, a consistency check of the SLH algorithm is performed, using CRM-simulated precipitation profiles as a proxy for the PR data. The algorithm-reconstructed heating profiles from CRM-simulated precipitation pro-

*Corresponding author address: Dr. Shoichi Shige, Department of Space Engineering, Osaka Prefecture University, 1-1 Gakuen-cho, Sakai, Osaka, 599-8531 Japan; e-mail: shige@aero.osakafu-u.ac.jp

files are compared to CRM-simulated "true" heating profiles, which are computed directly from the model thermodynamic equation. Here the 2-D version of the Goddard Cumulus Ensemble (GCE) model (Tao and Simpson, 1993) is used. Numerical simulations were conducted with the large-scale forcing data from TOGA-COARE, GATE, SCSMEX and KWAJEX. In this paper, the SLH algorithm is also applied to PR data and the results will be compared to heating profiles derived diagnostically from sounding data of SCSMEX (Johnson and Ciesielski, 2002). We will show the results with Q_1 - Q_R (Q_{1R}), which is the important dynamically important quantity. Here Q_1 is the apparent heat source defined in diagnostic studies (Yanai et al., 1973; Yanai and Johnson, 1993), and Q_R is the cooling/heating rate associated with radiative processes.

3. RESULTS AND DISCUSSIONS

3.1. *Consistency check of the original algorithm*

In addition to an episode from TOGA-COARE (19–26 December 1992) as shown in S2004, three episodes from GATE (September 1–8 1974), SCSMEX (June 2–9 1998) and KWAJEX (September 6–13 1999) are used for a consistency check of the SLH algorithm (Fig. 1).

The SLH1 algorithm with COARE lookup table produces excellent agreement between SLH-algorithm reconstructed and GCE simulated heating profiles for COARE (Fig. 1a), as shown in S2004. It may be noticed that the SLH1-reconstructed convective heating above the freezing level is slightly stronger than GCE-simulated one. This is because the simulated data used for the construction of lookup tables includes that from the two subperiods with 9-day durations (9–17 February 1993, and 18–26 February 1993) of which convection has stronger heating above the freezing level than that of the 19–26 December 1992 period. This is consistent with the result of DeMotte and Rutledge (1998a,b) who reported that convection of cruise 3 (29 Jan 1993–25 February 1993) has greater liquid and ice water masses above the freezing level than that of cruise 2 (21 December 1992–19 January 1993) using radar data.

On the other hand, the COARE lookup table produces less agreement between SLH1-reconstructed and GCE-simulated heating profiles for GATE convective and stratiform regions (Fig. 1b). The SLH1-reconstructed heating at z = 4–6 km is stronger than the GCE model-simulated one for convective heating profiles, while the SLH1 algorithm reconstructs cooling at z = 4–6 km where the GCE model simulates heating for stratiform heating profiles. The reconstructed total heating is in good agreement with simulated one. Compensation of error at z = 4–6 km for each component (convective and stratiform) is the reason for this good agreement. A separation of convective and stratiform heating profile estimates is very important, thus an algorithm improvement is needed.

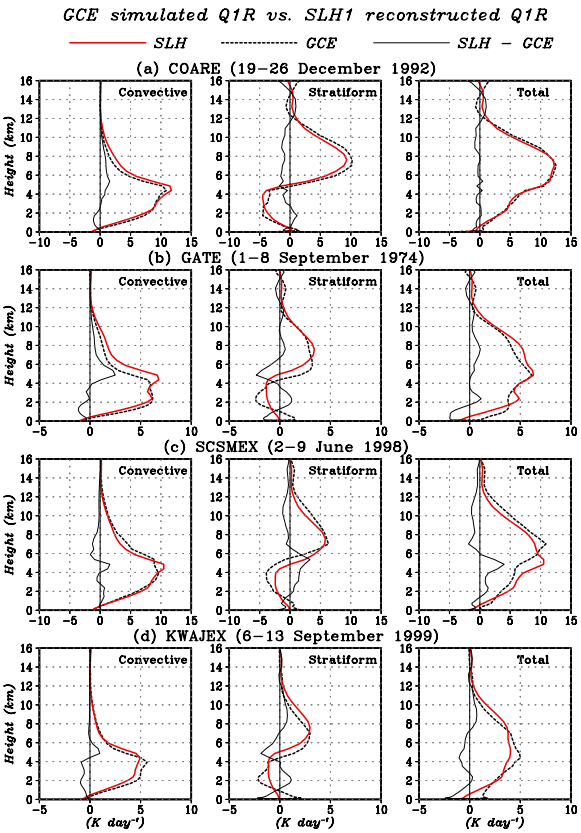

Figure 1: Eight-day averaged profiles of Q_{1R} reconstructed by the original SLH algorithm (SLH1) with the COARE lookup table (thick solid line) and simulated by the GCE model (dotted line) for (a) COARE (19–26 December 1992) case, (b) GATE (September 1–8 1974) case, (c) SCSMEX (June 2–9 1998) and (d) KWAJEX (September 6–13 1999), respectively. Left panels for convective regions, center panels for stratiform regions, and right panels for total regions. Thin solid line indicates differences between the SLH1-reconstructed and the GCE-simulated.

The COARE lookup table produces better agreement between reconstructed and simulated heating profiles for SCSMEX convective region than for GATE convective region (Fig. 1c). It is noticed that the SLH1-reconstructed convective heating decrease more rapidly with height above the freezing level than the GCE simulated one does, However, the reconstructed total heating is in poorer agreement with simulated one for SCSMEX than for GATE. The level of heating maximum of reconstructed total

heating profile is about 5 km, while that of simulated total heating profile is about 7 km. This is because the SLH1 algorithm reconstructs cooling at z = 4–6 km where the GCE model simulates heating for stratiform heating profiles and error for each component does not compensate.

The SLH1-reconstructed heating at z = 4–6 km is stronger than the GCE model-simulated one for KWAJEX total heating profile (Fig. 1d). This difference is mainly due to the disagreement between reconstructed and GCE simulated heating profiles for stratiform region where the SLH1 algorithm reconstructs cooling at z = 4–5 km where the GCE model simulates heating. Thus the algorithm improvement is needed for the stratiform region.

3.2. Comparisons of lookup tables

Figure 2a–d show lookup tables for convective rain produced from COARE, GATE, SCSMEX and KWAJEX simulations. The GCE-simulated precipitation profiles with a 0.3 mm h^{-1} precipitation-top threshold and corresponding heating profiles are accumulated and averaged for each PTH with model grid intervals. Two episodes from SCSMEX (18–26 May 1998 and 2–11 June 1998), two episodes from GATE (September 1–8 1974 and Sep 9–18 1974), and three episode KWAJEX (7–11 August 1999, 17–20 August, 29 August–5 September and 6–12 September) are used in order to increase the number of sample profiles.

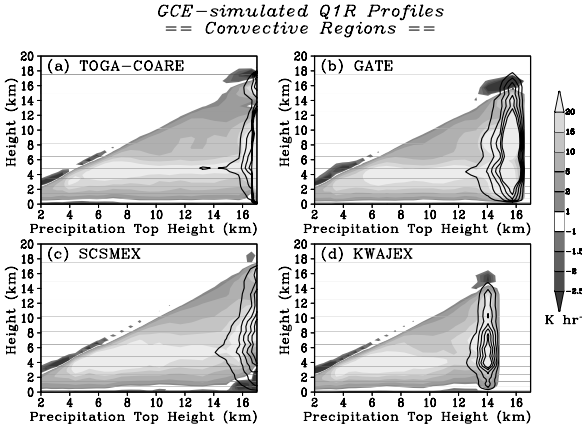

Figure 2: Ensemble-mean, GCE-simulated Q_{1R} profiles, plotted as functions of precipitation top height (PTH) from convective regions for (a) COARE, (b) GATE, (c) SCSMEX, and (d) KWAJEX cases. Contours indicate values of confidence interval for the mean at the 95 $\%$ level with Student's-t test. Contour interval is 2.0 K h^{-1}.

The similarity of lookup table from case to case can be seen. Properties of convective heating profiles show near-monotonic changes with PTH. The shallow convective heating profiles (PTH $<$ 6 km) are characterized by a cooling aloft due to an excess of evaporation over condensation, such as tradewinds cumulus (Nitta and Esbensen, 1974). Another interesting feature is that the convective heating profiles with highest PTH are characterized by a cooling aloft. This feature is consistent with strong cooling above the mesoscale convective system observed by Johnson and Kriete (1982) and Lin and Johnson (1996). On the other hand, there exists internal variations in vertical structure (e.g. the level of Q_{1R} heating maximum) for a given PTH. These accounts for the differences between the SLH1-reconstructed convective heating profiles and GCE-simulated ones seen in Fig. 1. Note that confidence level of heating profiles with PTH higher than 15 km (14 km) from GATE (KWAJEX) simulations for the mean is low because of the small number of profiles.

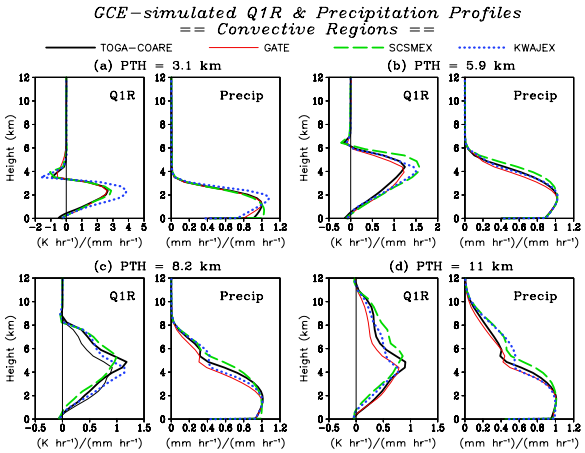

Figure 3: Ensemble-mean, GCE-simulated Q_{1R} and precipitation profiles, with precipitation top height (PTH) of (a) 3.1 km, (b) 5.9 km, (c) 8.2 km, and (d) 11km from convective regions for COARE, GATE, SCSMEX, and KWAJEX cases. Note that Q_{1R} profiles and precipitation profiles are normalized by near-surface rainrate.

Figure 3 shows GCE-simulated Q_{1R} and precipitation profiles, with precipitation top height (PTH) of 3.1 km, 5.9 km, 8.2 km, and 11km from convective regions for COARE, GATE, SCSMEX, and KWAJEX cases. Note that Q_{1R} profiles and precipitation profiles are normalized by near-surface rainrate. Heating top height is determined by PTH and the heating depth for a given PTH does not vary from location to location. The vertical structure (e.g., heating maximum level) of the shallow convective heating profiles (PTH = 3.1 km) does not vary from location to location. However, the differences in convective heating profile shape among cases increased with PTH. COARE convection provides stronger latent heating above the melting level than GATE and KWA-

JEX convection does, but weaker one than SCSMEX convection does. These differences are largest in the deeper convective heating profiles (PTH $>$ 8.2 km). These differences in the vertical distribution of deeper convective heating account for the discrepancies for convective region in the consistency check (Fig. 1).

Similarly, the differences in corresponding precipitation profile shape among cases also increased with PTH. COARE convection provides stronger precipitation intensity above the freezing level than GATE and KWAJEX convection does, but weaker one than SCSMEX convection does. Thus, the systematic variability of heating and precipitation profiles due to the relative importance of liquid water and ice processes is found above the freezing level. Convective cells with enhanced liquid water processes have latent heating and precipitation concentrated below the freezing level, whereas convective cells with significant ice processes provide stronger latent heating and more precipitation above the freezing level. Thus the precipitation profiles may be indicative of convective heating profile shape.

This is consistent with the results of Petersen and Rutledge (2001) who found the largest systematic variability in precipitation vertical structure between tropical locations above the freezing level using the TRMM PR and Lightning Imaging Sensor (LIS) observations. Furthermore, they pointed out that slight increases in convective intensity are present over South China Sea (i.e. SCSMEX) relative to isolated ocean regimes (i.e. COARE, GATE, KWAJEX) while convection over western Pacific warm pool (i.e. COARE) is slightly more intense than that sampled over other ocean (i.e. GATE, KWAJEX). Thus, the aforementioned differences among COARE, GATE, SCSMEX, and KWAJEX may be consistent with their results.

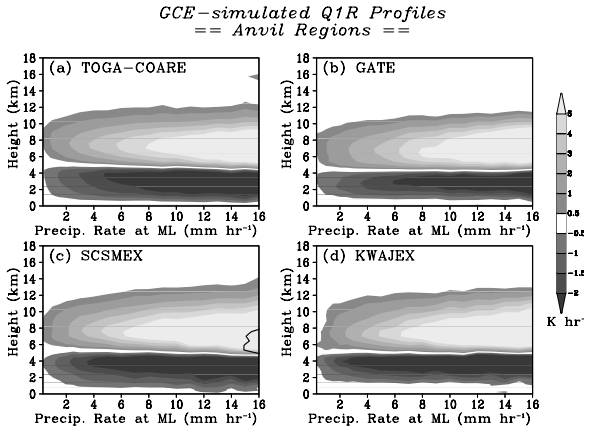

Figure 4: Lookup tables for the stratiform region produced from (a) COARE, (b) GATE, (c) SCSMEX and (d) KWAJEX simulations.

Fig. 4a–d show lookup tables for anvil (deep stratiform with a melting level) rain produced from COARE, GATE, SCSMEX and KWAJEX simulations. The similarity of anvil heating profiles among lookup tables from case to case can be seen, although there are differences of the level separating upper-level heating and lower-level cooling due to those of the melting level. These results agree well with observations of stratiform heating profiles summarized in Houze (1989) who concluded that stratiform heating profiles are not substantially different form one location to the next.

3.3. Algorithm improvements

Comparisons of convective lookup tables suggested that the variability of heating profiles above the freezing level should be taken into account for convective heating retrieval. Hence, upper-level heating amplitude due to ice processes and lower-level heating amplitude due to liquid water processes are determined separately in the revised procedure of convective heating retrieval (Fig. 5). Based on some sensitivity tests, the level separating upper-level heating and lower-level heating is determined that 1 km above the melting level.

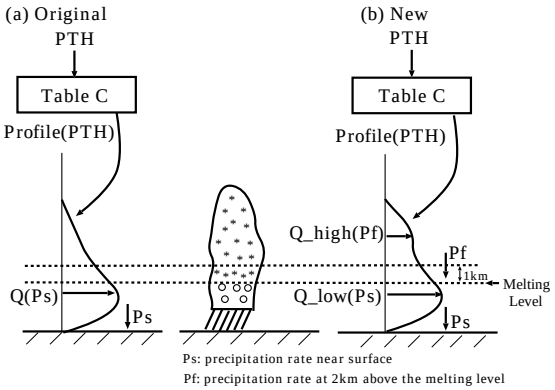

Figure 5: Diagram showing the procedure for deriving convective heating profiles using the spectral latent heating (SLH) algorithm. See the text for details.

The upper-level heating due to ice processes is determined by

$$Q(z)_{high} = \frac{\widetilde{Q}_{high}(z)}{\widetilde{P}_f} \cdot P_f. \qquad (1)$$

where P_f is the precipitation rate at the level separating upper-level heating and lower-level heating and tildes denote the variables in the lookup table. On the other hand, the lower-level heating due to liquid water processes is determined by

$$Q(z)_{low} = \frac{\widetilde{Q}_{low}(z)}{\widetilde{P}_s} \cdot P_s, \qquad (2)$$

where P_s is the precipitation rate at the observable lowest level. This revised procedure shown in Fig. 5b is only applied to convective rain with PTHs which are 3 km higher than the level separating upper-level heating and lower-level heating. The original procedure shown in Fig. 5a is applied to the remaining convective rain.

For stratiform regions, we shift up or down the heating profile by matching the melting level of COARE lookup table with observed one.

3.4. Consistency check of the revised algorithm

Again, the four episodes from TOGA-COARE (19–26 December 1992), GATE (September 1–8 1974), SCSMEX (June 2–9 1998) and KWAJEX (September 6–13 1999) are used for a consistency check of the revised SLH algorithm (SLH2), as shown in Fig. 6.

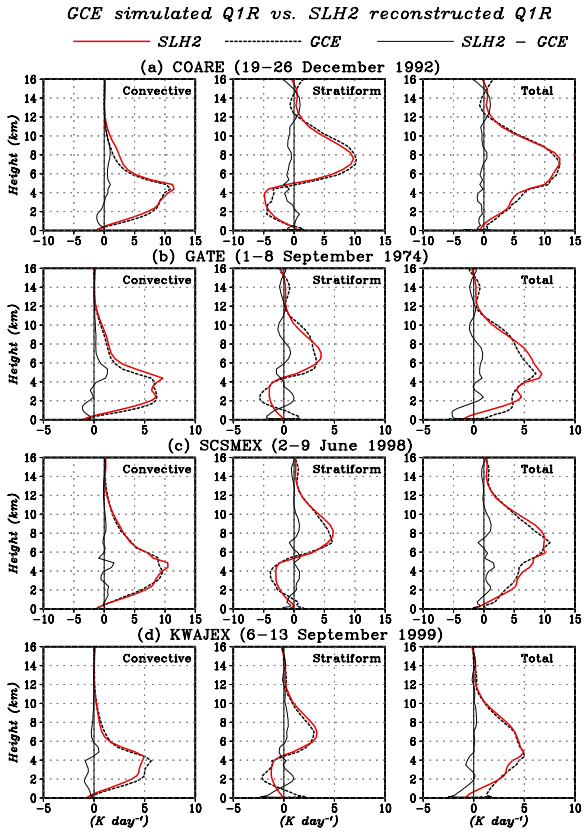

Figure 6: Same as Fig. 1, but reconstructed by the revised SLH algorithm (SLH2) with the COARE lookup table and simulated by the GCE model. Thin solid line indicates differences between the SLH2-reconstructed and the GCE-simulated.

For the COARE episode, the SLH2-reconstructed heating profiles for convective, stratiform, and total regions are almost identical to those reconstructed by the SLH1 algorithm. Actually, the SLH2-reconstructed heating profile for stratiform region is totally the same with the SLH1-reconstructed one, because adjustment of the melting level is not needed. Still, it is noticed that the SLH2 algorithm produces slightly weaker convective heating at z = 5–6.5 km than the SLH1 algorithm does and better agreement with the GCE model.

Although total heating profile reconstructed by the SLH2 algorithm is almost identical to that reconstructed by the SLH1 algorithm for the GATE episode, error for each component is reduced. For convective region, the SLH2 algorithm produces weaker heating above z = 5 km than the SLH1 algorithm does and much better agreement with the GCE model. For stratiform region, the discrepancy between the level separating upper-level heating and lower-level cooling reconstructed by the SLH2 algorithm and that simulated by the GCE model is reduced.

For the SCSMEX episode, the SLH2 algorithm produces stronger heating above z = 5 km than the SLH1 algorithm does, differed from the COARE and GATE episodes, and very good agreement with the GCE model. For stratiform region, the discrepancy between the level separating upper-level heating and lower-level cooling reconstructed by the SLH2 algorithm and that simulated by the GCE model is reduced and the very good agreement between heating profile reconstructed by the SLH2 algorithm and that simulated by the GCE model is obtained. As a result of improvements of convective and stratiform estimates, the total heating profile reconstructed by the SLH2 algorithm is in very good agreement with that simulated by the GCE model. The level of heating maximum reconstructed by SLH2 agrees with the GCE-simulated one.

For the KWAJEX episode, the better agreement between total heating profile reconstructed by the SLH2 algorithm and that simulated by the GCE model is explained by the fact that the discrepancy between the level separating upper-upper-level heating and lower-level cooling reconstructed by the SLH2 algorithm and that simulated by the GCE model is reduced for stratiform region. It is also noticed that the SLH2 algorithm produces slightly weaker convective heating at z = 5–6 km than the SLH1 algorithm does and better agreement with the GCE model.

3.5. Validation with SCSMEX-NESA radiosonde networks

The accuracy of SLH-retrieved heating can be evaluated by comparison with sounding-based heating for the SCSMEX NESA derived by Johnson and Ciesielski (2002). Figure 7 shows a comparison between SLH-retrieved Q_{1R} from PR Ver.6 data and sounding-based Q_1 during the campaign's most con-

vectively active period (May 15 - Jun 20 1998). There is good agreement insofar as various key features of the vertical profiles, particularly concerning the level of maximum heating. The SLH-retrieved Q_{1R} heating magnitudes are somewhat greater than the sounding-derived magnitudes. Tao et al. (2004) reported that the net radiation (cooling) accounts for about 20 % or more of the net condensation for the SCSMEX cloud systems simulated by the GCE model. Thus, the difference is mainly caused by the fact the SLH-retrieved Q_{1R} does not includes Q_R implied by the sounding-derived Q_1.

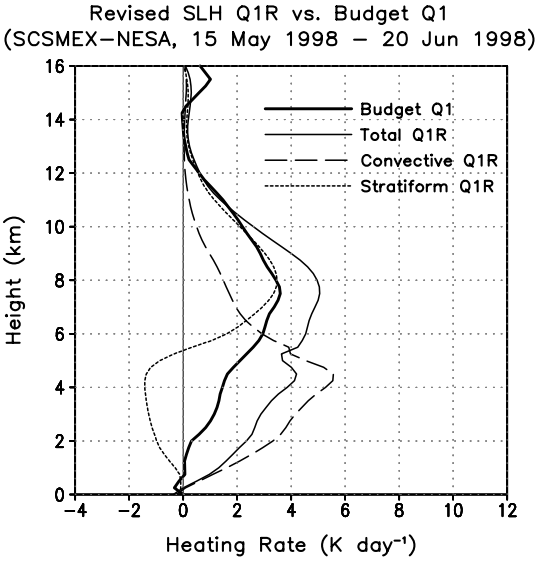

Figure 7: Heating from diagnostic calculations (Johnson and Ciesielski, 2002) and SLH algorithm for the SCSMEX NESA region (15 May - 20 June 1998).

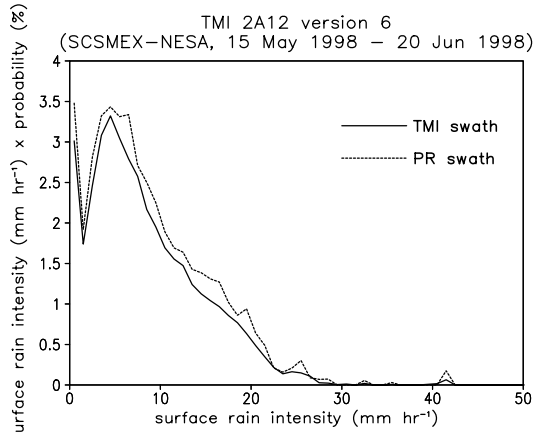

Figure 8: Contribution to total rainrate against the surface rain intensity estimated TMI 2A12 version 6 over within the PR swath and with TMI full swath.

The heating estimates from PR data are subject to sampling errors due to PR's narrow swath width (220 km), leading to a discrepancy with the sounding estimates. Figure 8 presents histogram of surface rainrates estimated TMI 2A12 version 6 over within the PR swath and with TMI full swath. The occurrences of moderate-to-heavy rain rates (≥ 5 mm h^{-1}) are more for the PR swath than for the TMI swath. Thus, sampling errors may partially account for the discrepancy with the sounding estimates shown in Fig. 7.

4. SUMMARY

In this study, the universality of the lookup table produced from COARE simulations of the SLH algorithm (Shige et al., 2004) was examined for its global application to TRMM PR data. We reconstructed heating profiles from CRM-simulated parameters (i.e. PTH, precipitation rate at the melting level, rain rate and type) with the COARE table and compared them to CRM-simulated " true " heating profiles, which were computed directly the model thermodynamic equation. The GATE, SCSMEX, and KWAJEX episodes were used for a consistency check.

The consistency check indicates that the COARE table produces discrepancies between the SLH-reconstructed and GCE-simulated heating above the melting level for convective region and at the melting level for stratiform region. Comparisons of the COARE lookup table with those from GATE, SCSMEX, and KWAJEX simulations show that the discrepancies for convective region are explained by differences in the vertical distribution of deeper convective heating due to the relative importance of liquid water and ice processes that varies from case to case. On the other hand, the discrepancies for stratiform region are explained by differences of the level separating upper-level heating and lower-level cooling due to those of the melting level.

Based on these results, algorithm improvements have been made to the SLH algorithm. In the revised procedure of convective heating retrieval, upper-level heating amplitude due to ice processes and lower-level heating amplitude due to liquid water processes are determined separately. For stratiform regions, we shift up or down the heating profile by matching the melting level of COARE lookup table with observed one. A consistency check indicates the revised SLH algorithm has a much better performance for each component (convective and stratiform) than the original one.

The revised SLH algorithm was also applied to PR data and the results was compared to heating profiles derived diagnostically from sounding data of SCSMEX (Johnson and Ciesielski, 2002). There is a good agreement insofar as various key features of the vertical profiles, particularly concerning the level of maximum heating. The SLH-retrieved Q_{1R} heating magnitudes are somewhat greater than the

sounding-derived magnitudes. This is basically consider to be caused by the fact the SLH-retrieved Q_{1R} does not includes Q_R implied by the sounding-derived Q_1. The discrepancy with the sounding estimates is partially explained by the fact that the heating estimates from PR data are subject to sampling errors due to PR's narrow swath width (220 km).

Acknowledgement This study is supported by the JAXA/EORC Tropical Measuring Mission (TRMM) project. The first author are grateful to Mr. Ken'ichi Ito and Mr. Masahiko Numata of RESTEC for helpful computing assistance and to Mr. Hiroshi Sasaki of Osaka Prefecture University for preparing TRMM data. Yukari N. Takayabu would like to express her hearty gratitude to late Prof. Tsuyoshi Nitta for motivating her to develop the latent heating algorithm utilizing TRMM PR data. W.-K. Tao and C.-L. Shie are mainly supported by the NASA headquarters Atmospheric Dynamics and Thermodynamics Program and the NASA TRMM. They thank Dr. R. Kakar at NASA headquarters for his support. The Grid Analysis and Display System (GrADS) package was utilized for the figures.

REFERENCES

Awaka, J., T. Iguchi, and K. Okamoto: 1998, Early results on rain type classification by the Tropical Rainfall Measuring Mission (TRMM) precipitation radar. *Proc. 8th URSI Commission F Open Symp.*, URSI, Aveiro, Portugal, 143–146.

Houze, R. A., Jr.: 1982, Cloud clusters and large-scale vertical motions in the tropics. *J. Meteor. Soc. Japan*, **60**, 396–410.

— 1989, Observed structure of mesoscale convective systems and implications for large-scale heating. *Quart. J. Roy. Meteor. Soc.*, **115**, 425–461.

Iguchi, T., T. Kozu, R. Meneghini, J. Awaka, and K. Okamoto: 2000, Rain-profiling algorithm for the TRMM precipitation radar. *J. Appl. Meteor.*, **39**, 2038–2052.

Johnson, R. H. and D. C. Kriete: 1982, Thermodynamic and circulation characteristics of winter monsoon tropical mesoscale convection. *Mon. Wea. Rev.*, **110**, 1898–1911.

— and G. S. Young: 1983, Heat and moisture budgets of tropical mesoscale anvil clouds. *J. Atmos. Sci.*, **40**, 2138–2146.

— and P. E. Ciesielski: 2002, Characteristics of the 1998 summer monsoon onset over the northern South China Sea. *J. Meteor. Soc. Japan*, **80**, 561–578.

Kozu, T., T. Kawanishi, H. Kuroiwa, M. Kojima, K. Oikawa, H. Kumagai, K. Okamoto, M. Okumura, H. Nakatsuka, and K. Nishikawa: 2001, Development of precipitation radar onboard the Tropical Rainfall Measuring Mission (TRMM) satellite. *IEEE Trans. Geosci. Remote Sens.*, **39**, 102–116.

Lin, X. and R. H. Johnson: 1996, Kinematic and thermodynamic characteristics of the flow over the western Pacific warm pool during TOGA COARE. *J. Atmos. Sci.*, **53**, 695–715.

Nitta, T. and S. Esbensen: 1974, Heat and moisture budget analyses using BOMEX data. *Mon. Wea. Rev.*, **102**, 17–28.

Okamoto, K.: 2003, A short history of the TRMM precipitation radar. *Cloud Systems, Hurricanes and The Tropical Rainfall Measurement Mission (TRMM): A Tribute to Dr. Joanne Simpson*, Meteor. Monogr, No. 51, Amer. Meteor. Soc., 187–195.

Petersen, W. A. and S. A. Rutledge: 2001, Regional variability in tropical convection: Observations from TRMM. *J. Climate*, **14**, 3566–3586.

Shige, S., Y. N. Takayabu, W.-K. Tao, and D. E. Johnson: 2004, Spectral retrieval of latent heating profiles from TRMM PR data. Part I: Development of a model-based algorithm. *J. Appl. Meteor.*, **43**, 1095–1113.

Takayabu, Y. N.: 2002, Spectral representation of rain features and diurnal variations observed with TRMM PR over the equatorial area. *Geophys. Res. Lett.*, **29**, doi:10.1029/2001GL014113.

Tao, W.-K., D. Johnson, C.-L. Shie, and J. Simpson.: 2004, The atmospheric energy budget and large-scale precipitation efficiency of convective systems during TOGA COARE, GATE, SCSMEX, and ARM: Cloud-resolving model simulations. *J. Atmos. Sci.*, **61**, 2405–2423.

— and J. Simpson: 1993, Goddard cumulus ensemble model. Part I: Model description. *Terr. Atmos. Oceanic Sci.*, **4**, 35–72.

Yanai, M. and R. H. Johnson: 1993, Impacts of cumulus convection on thermodynamic fields. *The Representation of Cumulus Convection in Numerical Models*, Meteor. Monogr., No. 46, Amer. Meteor. Soc., 39–62.

—, S. Esbensen, and J.-H. Chu: 1973, Determination of bulk properties of tropical cloud clusters from large-scale heat and moisture budgets. *J. Atmos. Sci.*, **30**, 611–627.